Ceramics International 49 (2023) 21538–21545

Contents lists available at ScienceDirect

Ceramics International

journal homepage: www.elsevier.com/locate/ceramint

The effect of Mo_2C additions on the oxidation resistance of (Ti,W)CN cermets as base material for the production of cutting tools

Morteza Hadi [a,*], Seyed Mahdi Rafiaei [a], Filipe Fernandes [b,c]

[a] Materials Engineering Group, Golpayegan College of Engineering, Isfahan University of Technology, 87717-67498, Golpayegan, Iran
[b] ISEP - School of Engineering, Polytechnic of Porto, Rua Dr. António Bernardino de Almeida 431, 4200-072, Porto, Portugal
[c] University of Coimbra, CEMMPRE - Centre for Mechanical Engineering, Materials and Processes, Department of Mechanical Engineering, Rua Luís Reis Santos, 3030-788, Coimbra, Portugal

ARTICLE INFO

Handling Editor: Dr P. Vincenzini

ABSTRACT

The effect of Mo_2C secondary carbide on the oxidation resistance of $(Ti_{0.93}W_{0.07})CN_{0.3}$-20%Ni cermet was investigated using DSC-TG, isothermal oxidation, XRD, and SEM/EDS characterisations. Adding Mo_2C secondary carbides to (Ti, W)CN cermets is one of the methods used for improving their mechanical properties. However, Mo_2C secondary carbides bring a detrimental effect to oxidation resistance. The isothermal oxidation results of the samples at 750 °C possessing 0% and 2% MO_2C follow the parabolic law, while in the samples containing 5% and 8% Mo_2C, the rate of oxidation and the spallation of the oxide scale increased significantly. The thickness of the oxide layer in the cermet containing 5% of Mo_2C increased three times, whereas the mass per unit area of the detached oxides in the 8% Mo_2C specimen dramatically increased up to 100 times. The investigations revealed that the increase in the amount of W and Mo on the cermet material, as well as the formation of a multi-zone oxide layer, are the main reasons for oxide phase propagation.

1. Introduction

With the development of demanding materials of better mechanical properties, new machining tool materials are required in many industrial machining processes [1–4]. Despite the efforts for improving the properties of WC-based cermet materials, they are not still able to meet the required properties, including hardness and oxidation resistance during operation [5]. Ti(C,N) cermet materials have been a suitable alternative to tungsten-based cermets for machining applications such as high-speed milling for finishing operations of stainless and carbon steel parts. For the past ten years, there has been a rapid rise in the efforts to modify the properties of the Ti(C,N) cermets [6–8]. Among these, studies focusing in the influence of refractory elements such as Tungsten, Tantalum, Niobium, and Molybdenum were substantial. Significant enhancement in mechanical properties develop a core-rim microstructure after the sintering could be achieved [9,10]. Secondary carbides such as WC, TaC, NbC, and Mo_2C restrict the grain growth during the sintering process at high temperatures, improving the mechanical properties [11,12]. For instance the modification of Ti(C,N) cermet material by adding WC has been successful in improving both fracture toughness and hardness [13,14].

On one hand, studies on the properties of different binders were also conducted for this type of cermets. Generally, nickel metal has been introduced as the conventional binder in Ti(C,N) investigations. Recently, researchers have reached impressive achievements on carbonitride cermets by adding Mo_2C to (Ti,W)C,N cermets [15,16]. It has been found that the hardness of $(Ti_{0.93}W_{0.07})CN_{0.3}$-Ni cermet could increase from 12.7 to 13.9 GPa by adding 8% of Mo_2C without a significant drop in fracture toughness [16]. However, these researchers have only focused their research on the cermets' microstructure, hardness, and fracture toughness. Nevertheless, the oxidation resistance of those materials has not yet been reported, as an important property to communicate since it also accounts for the good performance of the material in service. According to the published reports on Ti(C,N)-based cermets with the composition of Ti(C,N)-WC-Mo_2C-NbC-10%Ni-10%Co, Ti(C,N)-WC-Mo_2C-NbC-NiCr-10%Ni-10%Co and [10] (Ti,Ta)$C_{0.5}N_{0.5}$-20%Co [17], these exhibited relatively high oxidation resistance above 600 °C, and their mass gain curves obey the parabolic evolution [10]. On the other hand, WC-based cermet materials above 650 °C show lower oxidation resistance, and their oxidation curves follow a linear evolution [10,18]. Meanwhile, several studies have been accomplished to improve the oxidation properties of Ti(C,N) cermets by

* Corresponding author.
E-mail address: m.hadi@iut.ac.ir (M. Hadi).

https://doi.org/10.1016/j.ceramint.2023.03.288
Received 6 February 2023; Received in revised form 21 March 2023; Accepted 29 March 2023
Available online 1 April 2023

Table 1
Samples designation and chemical composition.

Sample designation	Chemical composition (%wt)
M_0	$(Ti_{0.93}W_{0.07})CN_{0.3}$-20%Ni
M_2	$(Ti_{0.93}W_{0.07})CN_{0.3}$-2%$Mo_2C$-20%Ni
M_5	$(Ti_{0.93}W_{0.07})CN_{0.3}$-5%$Mo_2C$-20%Ni
M_8	$(Ti_{0.93}W_{0.07})CN_{0.3}$-8%$Mo_2C$-20%Ni

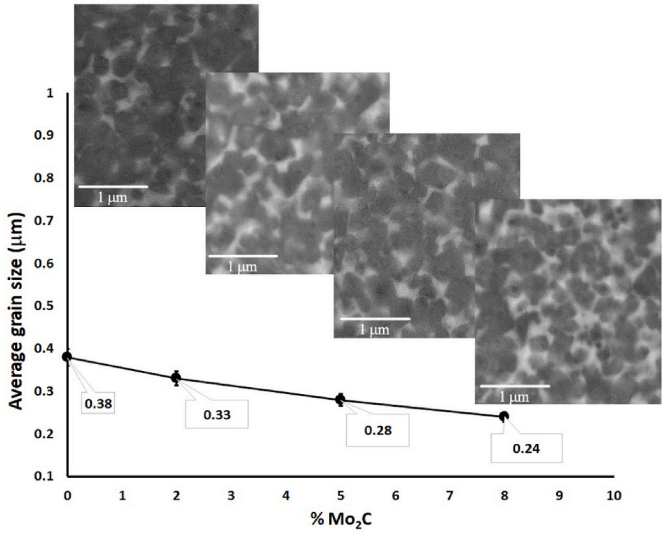

Fig. 1. Evolution of the grain size of the produced specimens as a function of the Mo_2C wt.%.

introducing other elements for improving their performance in the temperature range of 700-800 °C [5,19,20]. The primary importance of these articles is that the increase in temperature due to the application conditions can reduce the tool life. The investigations regarding increasing the hardness and mechanical properties of (Ti,W)CN-Ni cermets by adding Mo_2C can be completed by examining the effect of this additive on oxidation properties. As mentioned above, hardness and oxidation resistance are both essential in high-speed machining applications. Despite of this interest and to the best knowledge of the authors, no studies regarding the oxidation behaviour of $(Ti_{0.93}W_{0.07})CN_{0.3}$-$Mo_2C$-Ni cermets, which displayed improved mechanical properties have been reported in literature.

Therefore, the present research paper aims to investigate the oxidation resistance of $(Ti_{0.93}W_{0.07})CN_{0.3}$-(x)$Mo_2C$-Ni cermets, with different percentages of Mo_2C additions (x = 0, 2, 5, 8 wt%). In this regard, the cermets were isothermally tested for different times in an oven, their mass gain was continuously measured, and the amount of spallation of the oxide scale was compared. The surface and cross section morphology of the oxidised zone of the coatings was deeply characterised and the oxidation kinetics discussed.

2. Experimental details

$(Ti_{0.93}W_{0.07})CN_{0.3}$-20%Ni based cermet was synthesised according to the optimal method described in our previous study [15]. Herein, different cermet materials were produced via different amounts of Mo_2C secondary carbide (see Table 1). Disc type samples with a diameter of 10 mm were produced via uniaxial cold press under the pressure of 125 MPa. Then samples were sintered in a hot press set-up with optimal conditions (pressure of 0.13 Pa at 1510 °C for 1 h in a graphite mold). The sintering was done at this temperature since lower temperatures results in weak interfaces (between binder and carbides) and improper mechanical properties [15,16]. Thermogravimetric analysis-differential scanning calorimetry (TG-DSC, STD Q600 V 20.9) characterisations were conducted to continuously measure the mass changes. Also, the isothermally oxidation mass-gain measurements were performed at 750 °C for 50 h. The mass changes (including oxide spalls) were measured by using an AND balance with the preciseness of 10^{-1}mg. Following oxidation, the detached oxides were inspected by an X-ray diffractometer (XRD) with Cu-Kα radiation. Up-surface and cross section of specimens were observed by scanning electron microscopy (SEM, MIRA TE-Scan) equipped with energy-dispersive X-ray spectroscopy

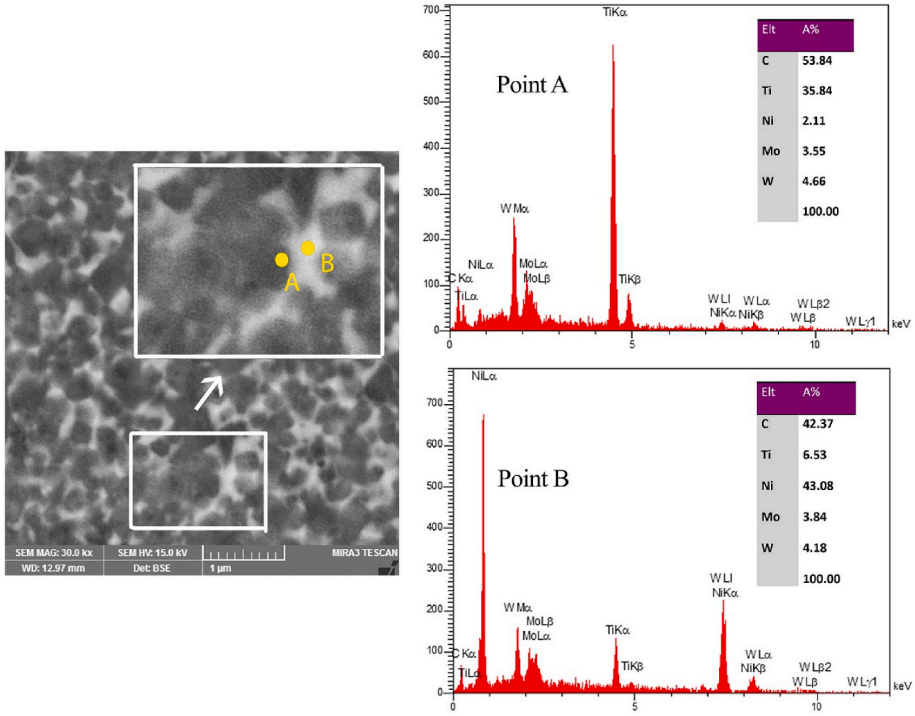

Fig. 2. SEM image and electron dispersive spectroscopy analysis conducted at the morphology of the surface of the M_8 sample.

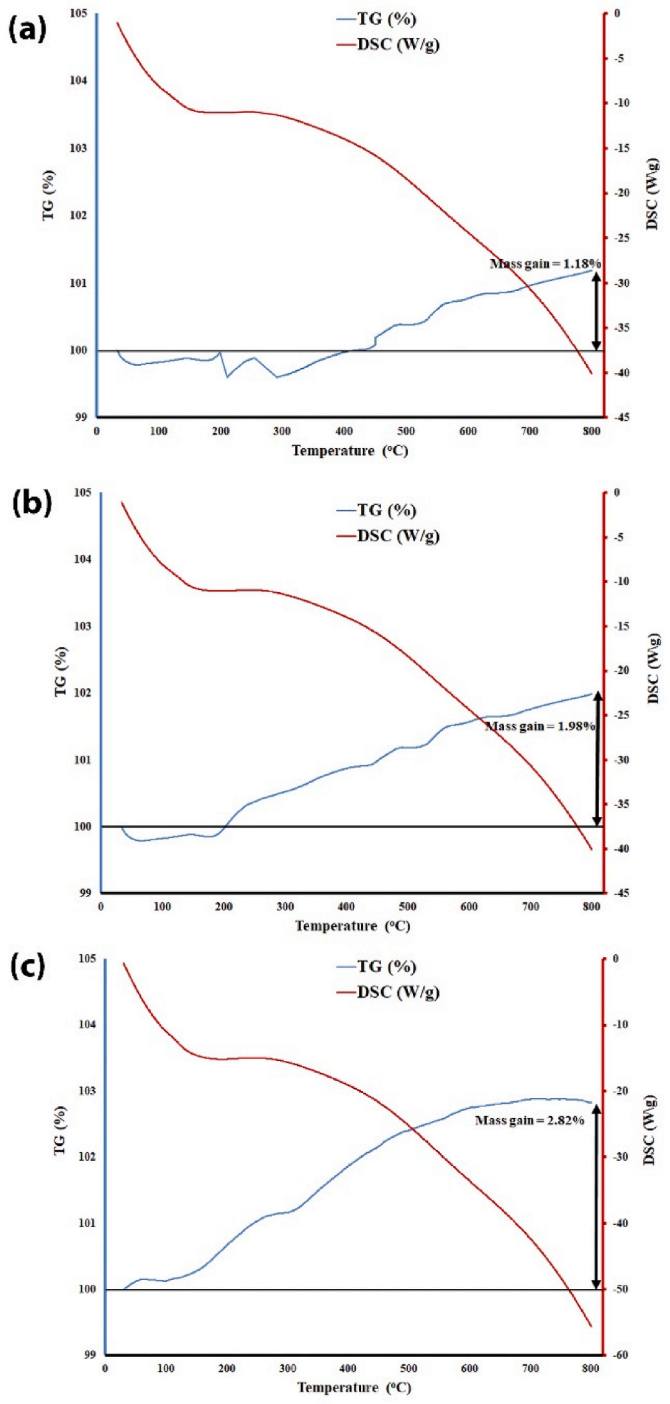

Fig. 3. DSC-TG curves of Mo_2C containing cermets (a) M_2, (b) M_5, and (c) M_8 with the temperature increasing up to 800 °C in an air atmosphere.

(EDS) before and after oxidation. The calculated average grain size of initial microstructures was determined by surveying at least 10 SEM images.

3. Results and discussions

3.1. Cermets' initial microstructure

Fig. 1 shows variation of the grain size of the studied cermets as a function of the Mo_2C concentration. In the chart an insert of the microstructure of each specimen is provided. As can be observed, the grain size of the specimens decreased almost linearly with the increase of Mo_2C concentration from 0.38 μm for the M_0 specimen to a minimum value of 0.24 for the M_8 specimen. This result is consistent with previous research in which the addition of Mo_2C caused the grain size refinement [11]. It has been found that secondary carbides with low solubility in the melted binder such as Mo_2C can lead to restrict increasing grain size during sintering of carbonitride cermets [16].

Furthermore, SEM-EDS examinations showed that compositional gradient formed in the microstructure of the specimens. Others have shown that these so-called core/rim structures are developed in the Ti(C, N)-based cermets as a consequence of various sintering steps [10]. A similar pattern of results was obtained in analysing the initial microstructure of specimens in this investigation. Fig. 2 shows the EDS analysis conducted at the two regions possible to distinguish on the material microstructure (grey regions and white areas) for the M_8 sample, representative of all the specimens. From the results, it is clear that in the rim zone adjacent to the binder (point A), is a phase rich in Ti, W, and Mo is formed. This result corroborates prior studies wherein the segregation of metal elements of carbides has occurred at the rim region due to different diffusion coefficients [12,15]. However, several EDS analyses of binder showed that significant amounts of tungsten and molybdenum dissolved in the nickel binders (Fig. 2). This result goes beyond previous reports [15], showing that in addition to the presence of molybdenum in the rim, the segregation of this element into the binder also occurs. The results also revealed that in the Mo_2C-containing samples, a substantial amount of tungsten was dissolved in the binder (See EDS of point B).

3.1.1. Oxidation behaviour

The data of TG-DSC examinations of Mo_2C-containing cermets are presented in Fig. 3. The DSC results of all specimens are all similar, suggesting that the phase stability of the cermets is not effectively influenced by Mo_2C addition. However, the TG curve shifted to the higher values and the mass gain at 800 °C increased through the addition of Mo_2C. This clearly revealed that the addition of Mo_2C reduced the oxidation resistance of the cermets. As the temperature increases, the slope of the TG curve decreases gradually suggesting that the oxidation of this cermet can be considered a multistage process in non-isothermal conditions. In previous research, it has been mentioned that the conversion of anatase-TiO_2 to Rutile-TiO_2 might be the reason for this behaviour [21]. Another explanation is in the very initial stage of oxidation, TiO_2 is a thin layer, and the interface reaction control the rate of oxidation. However, with progress in the oxidation process, diffusion in a relatively thick oxide layer control mass gain manner [22]. Therefore, the rate of oxidation decreased gradually.

In TG curves of non-oxide ceramics, the increase in weight is affected by oxygen incorporation, and the decrease in weight can be considered a result of the removal of moisture and gases created by oxidation reactions such as CO, H_2, $Ti(OH)_4$, etc. In other words, gas-solid interface reactions including oxidation and volatilization occur at high temperatures in these ceramics. As a result of the oxidation reaction of carbides, CO gas can be created, and oxidation with water vapor can lead to the release of H_2 gas or other volatile products such as $Ti(OH)_4$ [22]. The interaction between these two mechanisms in specimens M_2 and M_5 (Fig. 3-(a) and (b)) has caused a slight weight loss in the early stages and fluctuation in the curve. However, in sample M_8 (Fig. 3-(c)), where the oxidation rate is much higher, the phenomena of oxygen incorporation is dominant. Consequently, the weight loss resulting from removing oxidation gases has not been observed.

To get a better insight about oxidation resistance, isothermal oxidation tests were conducted. The aspect of the surface of the oxidised specimens exposed at 750 °C for 50 h are shown in Fig. 4. The progressive increase of the amount of yellow oxides grown in the surface of the base material with Mo_2C additions, clearly reveals a progressive loss of oxidation resistance of the base material. In addition, increasing the amount of Mo2C to ≥5% caused a significant increase in detaching of

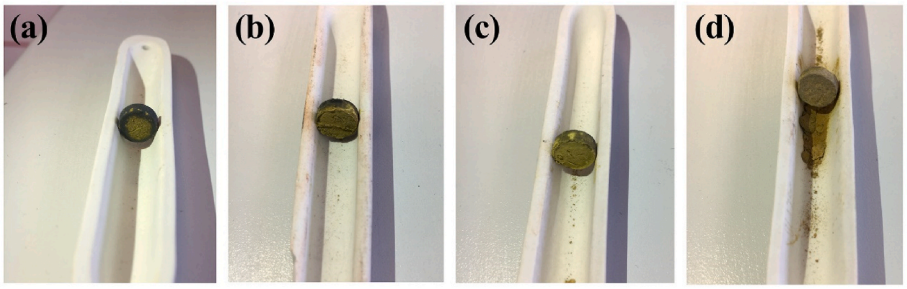

Fig. 4. A view of different specimens after oxidation at 750 °C for 50 h.

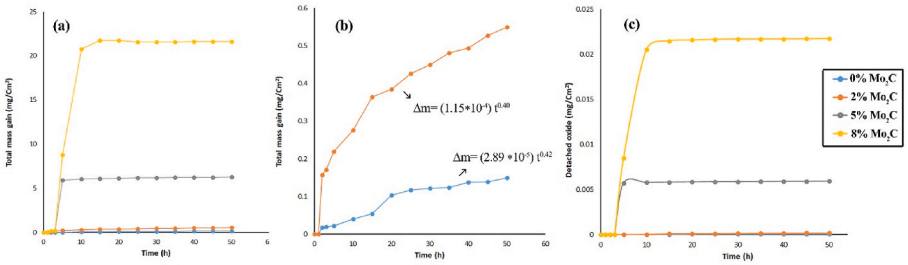

Fig. 5. Isothermal oxidation curves of the specimens tested in air at 750 °C for 50 h. (a) mass gain of all specimens (b) magnified mass gain curves of specimens contained 0 and 2% Mo_2C with curve fit results, and (c) mass of detached oxides versus time.

the oxide scale.

The isothermal oxidation resistance curves for the different specimens tested at 750 °C for 50 h are displayed in Fig. 5. The results show that the total mass gain in samples containing 5 and 8% Mo_2C (yellow and grey curves, respectively) had increased sharply at the early stage of oxidation and then became constant. The rate of mass gain due to the oxidation in samples M_5 and M_8 is so high that the increase in mass in samples M_0 and M_2 is not precipitable in a single graph. Therefore, the M_0 and M_2 curves are presented in a separate graph in Fig. 5-b. In this figure, the equations that arise from the parabolic behaviour evolution of the curves (typical equation $y = ax^b$ ($R^2 > 0.98$), representing the parabolic kinetics in the form of $\Delta m = kt^n$) are also shown. The exponential coefficient of specimens M_0 and M_2 (the values about 0.4) are very similarly to that of typical Ti(C,N) cermets [10]. The oxidation rate constant was 2.89×10^{-5} and 1.5×10^{-4} for specimens M_0 and M_2, respectively. This constant in Mo_2C-containg specimen is higher approximately 10 times suggesting that the mass gain increased remarkably. However, the mass gain trend in samples M_5 and M_8 does not match the parabolic evolution, even with the removal of large amounts of early time data ($R^2 < 1$).

The results show that after only 3 h, the oxidation behaviour of samples M_5 and M_8 had become entirely different, and the oxidation rate was significantly increased. Fig. 5-c also shows the increase in mass of the detached oxide of each specimen, which was precisely collected and weighed. Similarly, a significant difference is evident in these curves when comparing samples M_5 and M_8 with samples M_0 and M_2. The mass of detached oxides in M_8 is almost 100 times higher than that of M_0. The results of Fig. 5 are consistent with visual observations of the samples dealing with the amount of detaching oxide scale in Fig. 4. The very close matching of the curves of total mass gain and mass of the detached oxide indicates that the principal and controlling factor in the oxidation kinetics was the stripping of the oxide products from the samples. Weak adhesion and spallation of the oxide layer, particularly in M_5 and M_8 samples has intensified the oxidation so that after about 20 h, almost equivalent to the total weight added due to oxidation, the oxide products are separated from the cermets. The formation of pores and cracks and the exposure of the substrate to air due to the separation of the oxide scale causes the formation of faster penetration paths for anions and cations to diffuse which consequently accelerates the oxidation process [23]. The increase in the oxidation rate ceases after ~5 and ~20 h for M_5 and M_8 samples, respectively. It seems reasonable to assume that in instances with high Mo_2C addition, in the early stages, the selective oxidation of elements has changed the composition of the oxide layer; and as a consequence, the spallation of oxides has decreased. This conjecture, which explains the changes in the oxidation curves, can be verified by the micro-structural studies of the oxidised surface, which is discussed in the next section.

3.2. Oxidised surface

Fig. 6 shows the images of the oxidised surface of the reference M_0 sample without Mo_2C additions. It can be seen from the figure that the oxidised surface of this sample is not uniform and that it consists of two regions. Part of it has a yellow colour, and the other part is grey (Fig. 6-a). The fact that the SEM image of the sample with the backscatter electron detector (which is affected by the atomic number) has two zones, shows that the two regions with different colours observed in the actual image have two different compositions. Moreover from Fig. 6-(b) and (c), it is evident that the morphology of the two regions is also different. EDS analysis from one of the hillocks created at the oxide layer in the side zone (point A) shows that the area is rich in nickel oxide and has a small amount of Titanium oxide (Fig. 6-b). In contrast the analysis performed on one of the hills in the oxide layer in the second area (point B) shows that the amount of titanium oxide in this area increased considerably (Fig. 6-c).

The colour change from grey oxide in the first zone to yellowish oxide in the second zone corroborates the formation of high amounts of titanium oxide, which is usually pale yellow [24]. Since the samples were disc-shaped and were in contact with the container from the sides, it seems that the difference between the middle of the sample and its edge was that the middle was more exposed to air and oxidation. It is worth noting that the piece was taken out of the container for each weight measurement. Therefore, the possible rotations caused the oxidation to be slower at all the circular areas of the cermet edge than at the central region. This uneven exposure of the sample here can be worthwhile for the interpreting of the oxidation process. Considering the

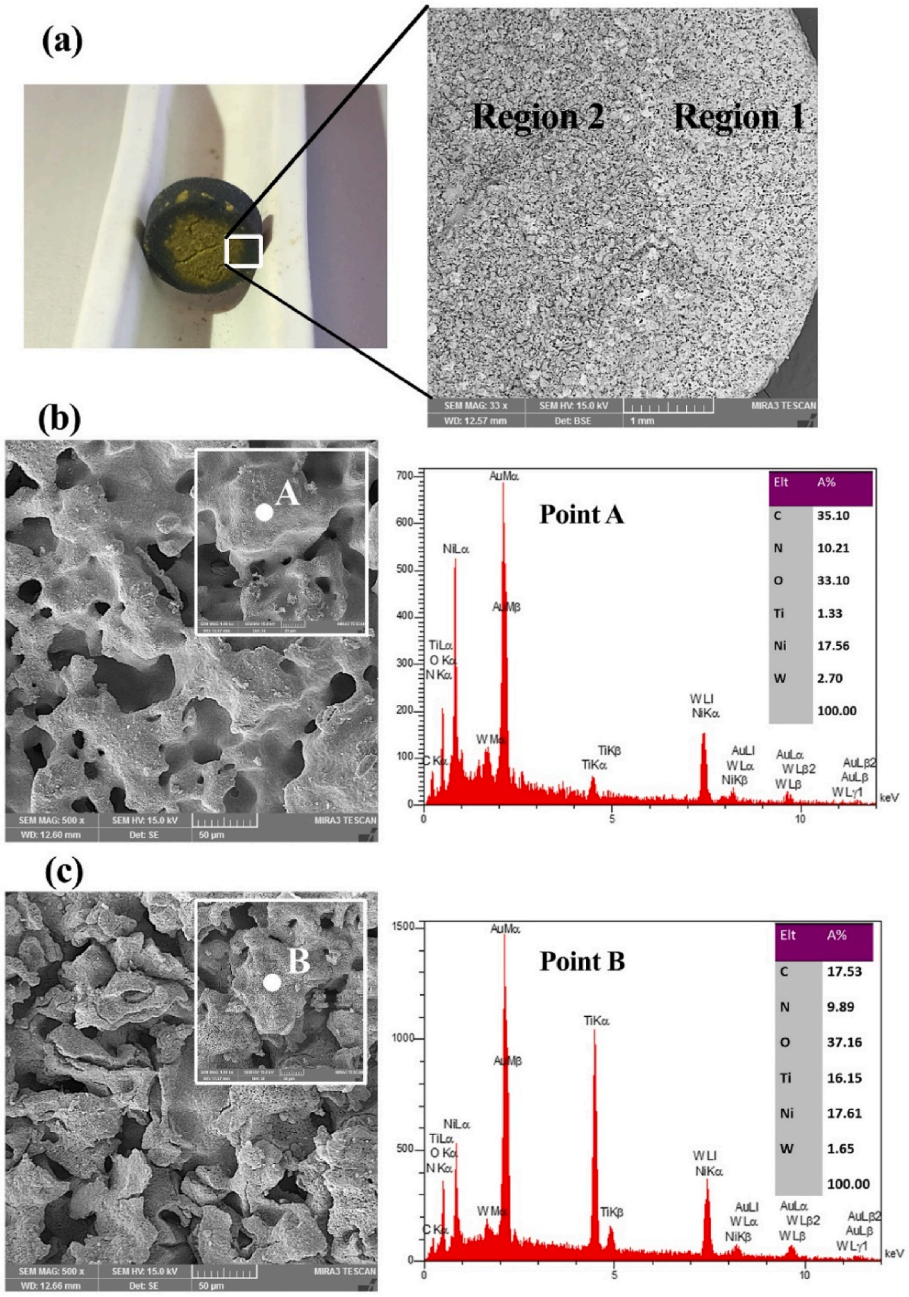

Fig. 6. Top surface morphology and EDS spectra of the oxidised surface of reference M_0 sample at (a) low magnification, (b) and (c) higher magnification at region 1 and 2, respectively.

points mentioned above, the results demonstrate two things: i) First, since the edge area of sample M_0 was less exposed than the center, due to contact with the container, it seems that this area represents earlier stages of the oxidation process. Meanwhile, the composition of another part of the specimen, which is more oxidised depicts the final stage of oxidation. Therefore, it can be concluded that the oxidation of these cermets starts with the formation of nickel oxide and is completed by further oxidation of titanium oxide. ii) Second, since the oxidation surface in the Mo_2C-free sample is not completely covered with yellowish oxide, it shows that this sample had a higher oxidation resistance than the Mo_2C-containing samples. This finding was also confirmed by the results obtained in accurate weight control (Figs. 4 and 5). Former studies showed that the formation of the oxide layer on the surface of Ti(C,N) carbides has three stages: (i) the first stage is the selective oxidation and growth of partial oxides; (ii) the second stage is to cover the entire surface with oxide; (iii) the last step is the orderly arrangement of oxide particles on the surface [10]. The results shown in Fig. 6 demonstrate that in primary stages of oxidation, nickel and tungsten are oxidised earlier than titanium. Since nickel is present in the composition of cermet as a binder and in elemental form; it oxidises earlier than other metals in a combined state. Moreover, between titanium carbide and tungsten carbide, the stability of tungsten carbide is lower (because the free energy formation of TiC is lower than that of WC [25]), which causes tungsten oxide to form earlier in the oxide scale. It could simply mean that the decomposition of titanium compounds in the cermets occurred at the final stages of oxidation. Therefore, titanium oxides formed through the penetration of ions (outward for titanium cations and inward for oxygen anions) within a pre-formed oxide layer. Other observations including cross-section examinations are in accordance with this claim which later discussed.

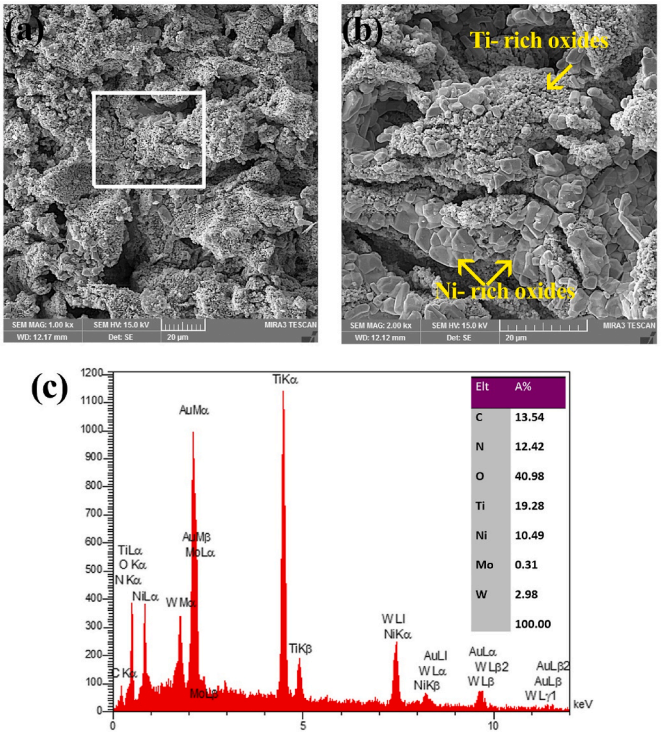

Fig. 7. SEM images and electron dispersive spectroscopy analysis conducted at the oxidised surface morphology of the M_2 sample.

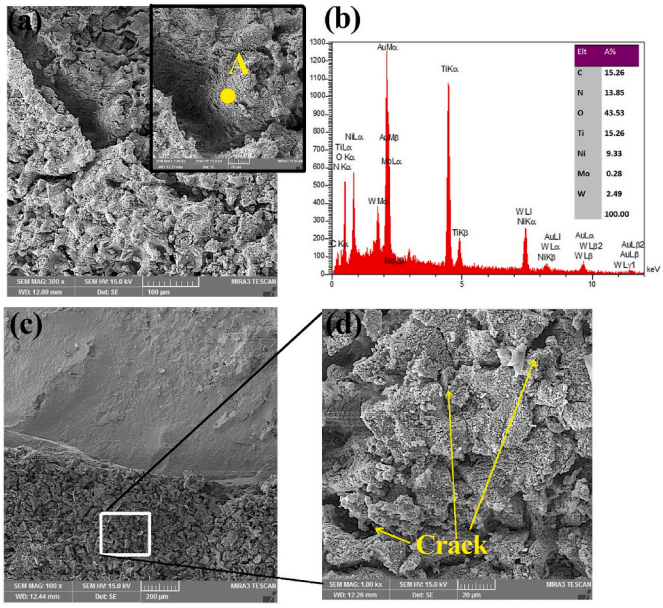

Fig. 8. (a) SEM image of a crack in the up surface of the M2 specimen, (b) EDS analysis of point A near to crack, (c) SEM image from the up surface of the M5 specimen, and (d) high magnification image of the area shown in part (c).

Fig. 7 shows the images of the oxidised surface of sample M_2 in two different magnifications and the corresponding EDS analysis. As seen in Fig. 2, unlike sample M_0, the entire outside is oxidised in this specimen, suggesting that the oxidation level is higher, in good agreement with the oxidation curves. The SEM morphology of the oxidised surface of sample M_2 is not similar to sample M_0 in any regions of 1 and 2. The results of EDS analysis of a large area representing the composition of the entire surface of the oxide scale is displayed in Fig. 7-c. Furthermore, the

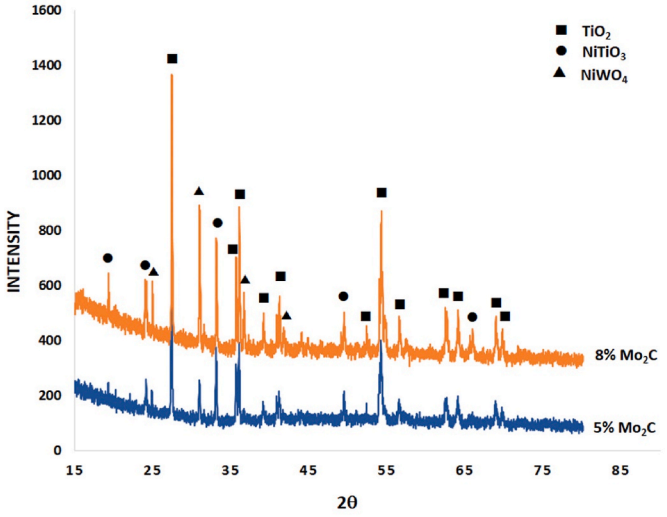

Fig. 9. XRD diffraction analysis of the detached oxide in specimens M_5 and M_8.

analysis of two different types of oxide observed in the oxide layer at higher magnification is marked with an arrow on the image (Fig. 7-b). The EDS results highlight that the amount of tungsten in the outer layer of the oxide scale in sample M_2 has reached 2.98 at%. However, in sample M_0, the amount of tungsten in the outer layer (region 2 in Fig. 6) was almost half of this quantity. In addition, molybdenum can be seen in the composition of the oxide scale of M_2, which was not present in the M_0 sample. Also, the comparison of the composition between M_0 and M_2 revealed that the amount of nickel in the M_2 sample has decreased in the outer layer of the oxide scale. It may suggest that changes in the oxide morphology of M_2 in comparison with M_0 occurred due to considerable compositional changes in the oxide scale. Previous studies on Ti(C,N) cermets showed that in the early stages of oxidation, a uniform $NiCo_2O_4$ layer is formed, which provides resistance to oxidation [10]. However, as seen in the microstructure of the oxide scale in sample M_2 (Fig. 7-(b)), the uniformity in the arrangement of nickel oxide particles with angular shapes is confined due to the presence of higher amounts of tungsten and titanium oxides. The importance of sample M_2 in this study is that the level of oxide detaching in this sample was lower than for instance in M_5 and M_8. Therefore, it is a suitable sample for exploring the compositional changes resulting from adding Mo_2C. In other words, M_2 represents the transitional conditions between the M_0 sample and the M_5 and M_8 samples.

Fig. 8-(a) shows an image of the cracks created in the oxide scale of sample M_2. Due to the low magnification image, the largeness of the crack can be recognized. These giant cracks, are an indication of the brittleness of the oxide scale with the addition of Mo_2C. The EDS analysis conducted in the area near these cracks (Fig. 8-b) shows that the amount of tungsten in the oxide scale of the sample containing 2% Mo_2C has increased. Meanwhile, according to several analyses, the composition of this zone is almost similar to that of the oxide scale in Fig. 7. This result confirms the fact that the addition of Mo_2C has restricted the process of forming a uniform and compact oxide scale. Accordingly, by changing the composition, the oxide scale in Mo_2C-containing cermet materials is transformed into a new mix oxide layer (Fig. 7-b) that is crispy and has cracks (Fig. 8-a).

The examinations, as will be discussed below, show that the changes made in the oxide layer of the M_2 sample are repeated and intensified in the M_5 and M_8 samples. Consequently, the stripping of the oxide scale from these samples increased remarkably (see Figs. 4 and 5). An image of the surface of sample M_5 is presented in Fig. 8-(c), where an area containing the remaining oxide scale and a region where the oxide scale has been detached can be seen. The remained oxide scale after significant loss of the oxide mass cannot be a definite representation of the

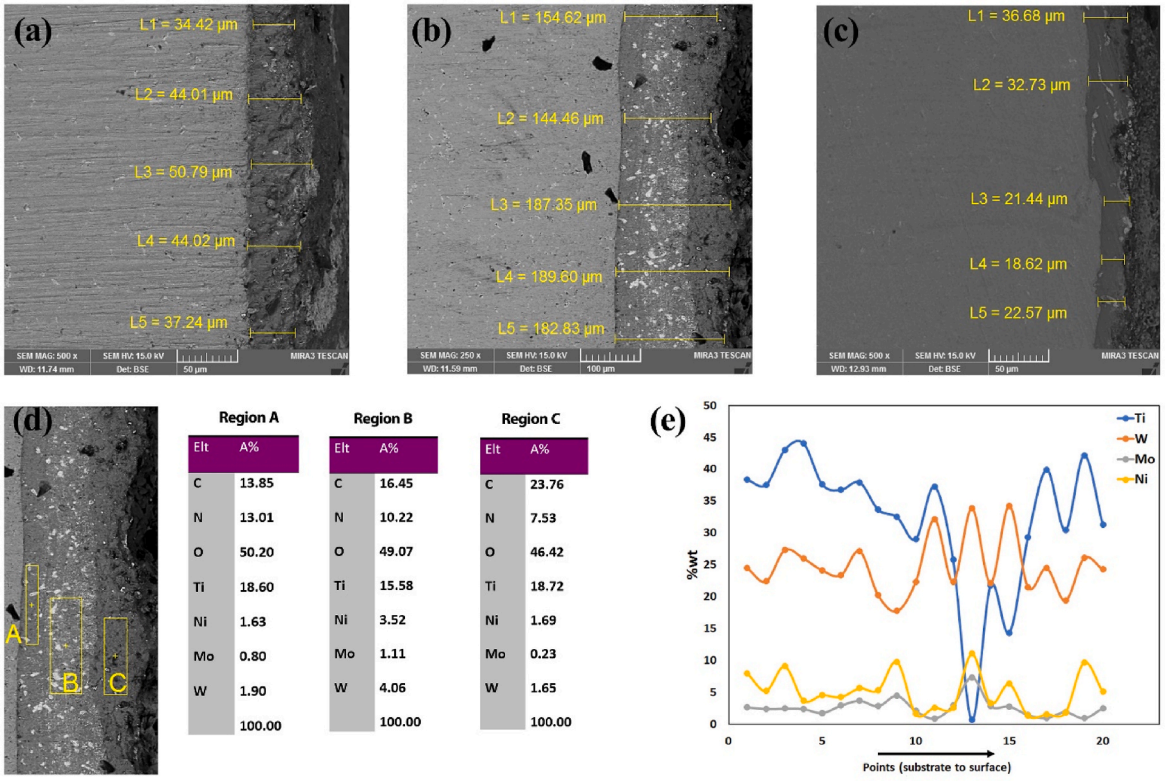

Fig. 10. (a), (b), and (c) Cross-section image of substrate/oxide interface of M_2, M_5, M_8 specimens, respectively. (d) bulk EDS analysis of three regions observed in M5 cross-section image, and (e) line-scan results of substrate to oxide acquired by twenty points EDS analysis in M_5 sample.

outer oxide layer in this sample. However, a comprehensive investigation of the remaining oxide layer also indicates that a compact oxide layer as expected in Ti(C,N) cermets is not formed and that many pores and cracks are inside the oxide scale (Fig. 8-(d)). As mentioned before, the excessive stripping of the oxide scale from the M_8 sample makes it practically impossible to examine and compare the changes in the morphology of the outer surface of the oxide.

Fig. 9 shows the XRD diffraction patterns of oxide scale detached from the M_5 and M_8 specimens. The rate of spallation in the M_0 and M_2 samples was minimal, and the amount of oxide stripped from these samples was insufficient for an XRD analysis. Since a significant difference concerning the mass of the detached oxide was observed between specimens M_0 and M_2 with M_5 and M_8, this XRD analysis is essential for the interpretation of oxidation. The result revealed that the TiO_2 phase is present in the pattern of both M_5 and M_8 samples as the primary phase. Also, nickel and titanium oxide (in the form of $NiTiO_3$) can be seen in the XRD patterns of the detached oxides of both samples. The presence of other complex oxide compounds such as $NiCoO_4$ previously reported for Ti(C,N) cermets [10], may also be presented, however, they are not detected by XRD due to their low quantity. Moreover, the $NiWO_4$ phase was also detected in the XRD pattern of the samples. Interestingly the peak intensity of this phase is enhanced in the specimen containing 8% Mo_2C. The most striking conclusion to emerge from this finding is that the increase of this complex oxide phase of nickel and tungsten has caused an increase in the spalling rate and consequently an increase in the oxidation rate. As can be seen from Fig. 9, the only change observed in the XRD patterns of M_5, and M_8 samples is the increase in the peak intensity of the $NiWO_4$ phase, which points to the likelihood that the rise in the oxidation rate was related to this phase. In the scrutiny of the upper surface of the oxide scale of the M_2 sample, where severe spallation did not occur, it revealed that with the addition of Mo_2C, the amount of tungsten in the oxide layer increases. This conformity in findings suggest that increasing the tungsten content of the oxide layer has caused the oxide scale to become brittle, particularly in the early stages of oxidation. The appearance of cracks caused by the brittleness of the scale has increased the diffusion and the oxidation rate. This can explain the significant rise of the curve of samples M_5 and M_8 compared to M_0 and M_2 (Fig. 5). However, with the formation of titanium oxide, the oxidation rate is restrained even in the M_5 and M_8 samples. Indeed, after a specific period of exposure time, the oxidation curves evolve a horizontal plateau.

Fig. 10 represents the oxidised cross-section of Mo_2C containing samples. As can be seen from the figure, by increasing the amount of the Mo_2C phase, the width of the oxide layer in the M_5 sample (Fig. 10-b) is approximately three times higher as compared to the M_2 specimen (Fig. 10-a). The image shown in Fig. 10-b is taken from the point in the M_5 specimen where the oxide layer is less detached. This enabled us to acquire a more precise estimate of the width of the oxide layer of sample M_5. However, this was not possible for the M_8 sample, and as seen from Fig. 10-c, where severe spallation leads to a lower width of the oxide layer. The most intriguing finding of the cross-section investigation was that in the remaining region of the oxide layer of sample M_5, there were three zones discerned, which had different compositions (Fig. 10-d). It seems that the difference observed in the amount of carbon on the surface, is caused by surface contamination of the outer surface of the sample. Crucially, comparing the composition of these three zones, the amount of W and Mo has risen in the median region. It was mentioned that the presence of W and Mo in the oxide layer may be responsible for the brittleness of the oxide scale, more spallation, and an increased oxidation rate. The result obtained in the cross-section analysis confirmed that increasing the amount of oxidation by adding Mo_2C was due to increasing these elements (W and Mo) in the oxide layer. In previous works, it has been stated that the oxidation of molybdenum-based compounds starts at 700 °C and reaches a maximum at 750 °C [26]. Fig. 10-(d) shows the segregation of these two elements in the middle layer of the oxide scale, which might be a multiplier reason for

higher brittleness and severe spallation. The line-scan analysis depicted in Fig. 10-(e) also confirms that the segregation of tungsten and molybdenum elements, which caused the increase in the oxidation rate, occurs in the center of the oxide layer. Furthermore, in this median region, the concentration of titanium decreases. This segregation restricts the uniform distribution of passive TiO_2 oxide throughout the oxide layer. It is noteworthy that in the analysis of the up-oxidised surface, due to the penetration depth of the electron beam in the SEM, it was impossible to specify that the segregation mentioned above occurred in the oxide layer. Therefore, the top surface analysis results only showed a rise in the amount of W and Mo elements in M_5 and M_8 samples. Nevertheless, the results of the cross-sectional study revealed that the brittleness and spallation of the oxide scale in instances M_5 and M_8 could result from the segregation occurring in the oxide layer and the non-uniform distribution of TiO_2. It is clear that with the passage of oxidation time, the activity of tungsten on the surface of the substrate gradually decreases, and as a result, oxidation of titanium prevails. Consequently, detaching of the oxide scale has also decreased. Finally, the formation of a uniform layer of titanium oxide has prevented severe oxidation similar to the initial time. In consolidation, when Mo_2C secondary carbide is added to the base material, progressive spallation of the oxide scale is observed with increasing Mo_2C concentration. This increases the mass gain rate since oxidation will be controlled by interface reaction and not by diffusion in the passive oxide layer. As mentioned above the presence of W and Mo in the oxide layer are the cause for the brittleness of the oxide scale, consequently leading to the oxides spallation and an increased oxidation rate.

4. Conclusions

The results of this research revealed that the oxidation resistance of (Ti,W)CN cermets progressive decreases with the increase of concentration Mo_2C secondary carbide. With the addition of Mo_2C, despite the favourable effects on the grain size and hardness of cermet, the composition of the oxide layer changes, leading to an increase in the oxidation rate. This research uncovered that cermets with up to 2% Mo_2C have a parabolic oxidation curve and the increase in oxidation rate is not severe. However, in cermets with 5 and 8% Mo_2C, forming a three-zone oxide layer containing higher amounts of W and Mo led to increased spallation. This behaviour was related to the formation of the $NiWO_4$ phase.

Declaration of competing interest

The authors declare that they have no known competing financial interests or personal relationships that could have appeared to influence the work reported in this paper.

Acknowledgements

Filipe Fernandes acknowledges the MCTool[21] - ref. “POCI-01-0247-FEDER-045940″ and CEMMPRE – ref. “UIDB/00285/2020” projects, sponsored by FEDER funds through the program COMPETE – Programa Operacional Factores de Competitividade – and by national funds through FCT – Fundação para a Ciência e a Tecnologia.

References

[1] L. Chen, D. Yi, B. Wang, H. Liu, C. Wu, X. Huang, H. Li, Y. Gao, The selective oxidation behaviour of WC–Co cemented carbides during the early oxidation stage, Corrosion Sci. 94 (2015) 1–5.
[2] H. Karimi, M. Hadi, Effect of sintering techniques on the structure and dry sliding wear behavior of WC-FeAl composite, Ceram. Int. 46 (2020) 18487–18497.
[3] A. Mostajeran, R. Shoja-Razavi, M. Hadi, M. Erfanmanesh, M. Barekat, M. S. Firouzabadi, Evaluation of the mechanical properties of WC-FeAl composite coating fabricated by laser cladding method, Int. J. Refract. Metals Hard Mater. 88 (2020), 105199.
[4] M. Hadi, H. Karimi, O. Bayat, I. Ebrahimzadeh, Influence of nanostructured FeAl powder addition on mechanical properties of WC composites produced by Spark plasma sintering technique, J. Sci. Technol. Compos. 6 (2019) 225–233.
[5] X. Kang, N. Lin, Y. He, M. Zhang, Influence of ZrC addition on the microstructure, mechanical properties and oxidation resistance of Ti (C, N)-based cermets, Ceram. Int. 44 (2018) 11151–11159.
[6] W. Lengauer, F. Scagnetto, Ti (C, N)-based cermets: critical review of achievements and recent developments, Solid State Phenom. 274 (2018) 53–100.
[7] M. Chen, Q. Zhuang, N. Lin, Y. He, Improvement in microstructure and mechanical properties of Ti (C, N)-Fe cermets with the carbon additions, J. Alloys Compd. 701 (2017) 408–415.
[8] M. Zhang, N. Lin, Y. He, X. Kang, A comparative study on microstructure and properties of Ti (C, N)-based cermets with the various Cr doping methods, J. Alloys Compd. 799 (2019) 462–473.
[9] X. Kang, Y. He, N. Lin, M. Zhang, Y. Yan, J. Huang, A study of the preparation and properties of dense binderless titanium carbonitride-based ceramics, J. Alloys Compd. 843 (2020), 155941.
[10] M. Zhang, Y. Jiang, N. Lin, X. Kang, Y. Yan, J. Huang, Y. Liu, S. Qiu, Y. He, Investigation of the oxidation behavior and high oxidation-resistant mechanism of Ti (C, N)-based cermets, Corrosion Sci. 177 (2020), 108959.
[11] C. Liu, N. Lin, Y. He, Influence of Mo2C and TaC additions on the microstructure and mechanical properties of Ti (C, N)-based cermets, Ceram. Int. 42 (2016) 3569–3574.
[12] P. Wu, Y. Zheng, Y. Zhao, H. Yu, Effect of TaC addition on the microstructures and mechanical properties of Ti (C, N)-based cermets, Mater. Des. 31 (2010) 3537–3541.
[13] L. Zhang, Q. Ling, J.-h. Gu, Z.-q. Zhong, J.-w. Long, C.-g. Wang, Strengthening and toughening of Ti (C, N)-based cermets:(Ti, W) C additive design and the mechanism, Int. J. Refract. Metals Hard Mater. 103 (2022), 105758.
[14] W.T. Kwon, J.S. Park, S.-W. Kim, S. Kang, Effect of WC and group IV carbides on the cutting performance of Ti (C, N) cermet tools, Int. J. Mach. Tool Manufact. 44 (2004) 341–346.
[15] S.M. Rafiaei, A. Bahrami, M. Shokouhimehr, Influence of Ni/Co binders and Mo2C on the microstructure evolution and mechanical properties of (Ti0. 93W0. 07) C–based cermets, Ceram. Int. 44 (2018) 17655–17659.
[16] S.M. Rafiaei, J.-H. Kim, S. Kang, Effect of nitrogen and secondary carbide on the microstructure and properties of (Ti0. 93W0. 07) C–Ni cermets, Int. J. Refract. Metals Hard Mater. 44 (2014) 123–128.
[17] E. Chicardi, J. Córdoba, F.J. Gotor, Kinetics of high-temperature oxidation of (Ti, Ta)(C, N)-based cermets, Corrosion Sci. 102 (2016) 168–177.
[18] H. Karimi, M. Hadi, I. Ebrahimzadeh, M.R. Farhang, M. Sadeghi, High-temperature oxidation behaviour of WC-FeAl composite fabricated by spark plasma sintering, Ceram. Int. 44 (2018) 17147–17153.
[19] H. Zhang, M. Fu, L. Ma, S. Gu, J. Liu, Y. Chen, Fabrication and properties of (Ti, W, Mo, Nb, Ta)(C, N)-Co-Ni cermets, J. Mater. Eng. Perform. 28 (2019) 7198–7205.
[20] C. Barbatti, J. Garcia, P. Brito, A.R. Pyzalla, Influence of WC replacement by TiC and (Ta, Nb) C on the oxidation resistance of Co-based cemented carbides, Int. J. Refract. Metals Hard Mater. 27 (2009) 768–776.
[21] C. Guo, X. Duan, Z. Fang, Y. Zhao, T. Yang, E. Wang, X. Hou, A new strategy for long-term complex oxidation of MAX phases: database generation and oxidation kinetic model establishment with aid of machine learning, Acta Mater. 241 (2022), 118378.
[22] E. Wang, X. Hou, Y. Chen, Z. Fang, J. Chen, T. Liang, K.-c. Chou, K.G. Nickel, Progress in cognition of gas-solid interface reaction for non-oxide ceramics at high temperature, Crit. Rev. Solid State Mater. Sci. 46 (2021) 218–250.
[23] H. Karimi, A. Ghasemi, M. Hadi, Microstructure and oxidation behaviour of TiAl (Nb)/Ti2AlC composites fabricated by mechanical alloying and hot pressing, Bull. Mater. Sci. 39 (2016) 1263–1272.
[24] M. Hadi, O. Bayat, M. Meratian, A. Shafyei, I. Ebrahimzadeh, Oxidation properties of a beta-stabilized TiAl alloy modified by rare earth elements, Oxid. Metals 90 (2018) 421–434.
[25] G. Song, Y. Zhou, Y. Wang, The microstructure and elevated temperature strength of tungsten-titanium carbide composite, J. Mater. Sci. 37 (2002) 3541–3548.
[26] E. Wang, Y. Guo, C. Guo, T. Yang, X. Hou, Z. He, H. Wang, Effect of temperature on the initial reaction behavior of MAB phases (MoAlB powders) at 700–1000° C in air, Ceram. Int. 47 (2021) 20700–20705.